JOURNAL OF GEOPHYSICAL RESEARCH, VOL. 105, NO. D20, PAGES 24,715–24,730, OCTOBER 27, 2000

Arctic polar stratospheric clouds observed with the Improved Limb Atmospheric Spectrometer during winter 1996/1997

Sachiko Hayashida, Naoko Saitoh, and Akiko Kagawa

Faculty of Science, Nara Women's University, Nara, Japan

Tatsuya Yokota, Makoto Suzuki,[1] Hideaki Nakajima, and Yasuhiro Sasano

National Institute for Environmental Studies, Tsukuba, Japan

Abstract. The newest retrieval (version 4.20) of the Improved Limb Atmospheric Spectrometer (ILAS) on board the Advanced Earth Observing Satellite (ADEOS) captured more than 60 polar stratospheric cloud (PSC) profiles during the winter and early spring of 1997 in the Northern Hemisphere. That winter is well known for its long-lasting polar vortex and significant ozone loss over the Arctic. The ILAS PSC measurements were the only spaceborne measurements made on a regular basis (about 14 times daily) during that period. PSC events were selected by comparing an individual profile with a threshold value at each altitude that was defined as an average of the extinction coefficient of background aerosols plus five standard deviations. Many of the selected PSC events correspond to temperatures lower than the nitric acid trihydrate (NAT) temperature, which was calculated using nitric acid and water vapor data observed with ILAS. The correlation between the aerosol extinction coefficient and temperature shows that the extinction data increase as the temperature decreases to a point several degrees lower than the NAT temperature, suggesting the formation of particles of a supercooled ternary solution. Some of the nitric acid profiles corresponding to intense PSC events showed a decreased mixing ratio, suggesting the uptake of nitric acid in the gas-phase into particles. The highest probability of sighting PSCs was obtained in mid-January at an altitude of approximately 23 km, and subsequent occurrences of PSCs were found intermittently at lower altitudes until mid-March. The 1997 Arctic winter was characterized by the prolonged appearance of PSCs until mid-March, associated with a long-lasting polar vortex. The PSC data presented in this paper compensate for the gap in the long-term PSC record from space and help to reveal the chemical mechanisms that caused the Arctic ozone loss observed that season.

1. Introduction

In the Arctic vortex, low column ozone values were observed in the late winter/spring in 6 of the last 10 years [*World Meteorological Organization (WMO)*, 1998]. It is recognized that polar stratospheric clouds (PSCs) play an important role in ozone destruction over the polar regions as a result of heterogeneous reactions occurring on their surface, which convert inactive reservoir chlorine into active chlorine [e.g., *Solomon*, 1990]. Recent stratospheric data show a trend in decreasing temperature [*WMO*, 1998]. Many studies have reported a decrease in the temperature over the Arctic. *Labitzke and van Loon* [1994] reported that between 1964 and 1993 the temperature in the lower stratosphere tended to decline. *Pawson and Naujokat* [1997] found that the area with T <195 K at 50 hPa has increased over the past 31 years, implying an increase in the frequency of PSC formation. *Waibel et al.* [1999] showed that conditions in the Arctic are at the threshold for denitrification. A temperature decrease of 1° would enhance PSC formation, which might cause significant denitrification and therefore significant ozone loss over the Arctic.

Currently, it is of scientific interest to determine any trend in the frequency of PSCs. PSCs have been observed from space [*Poole and Pitts*, 1994; *Fromm et al.*, 1997], with ground-based and airborne lidars

[1]Now at Earth Observation Research Center, National Space Development Agency, Tokyo, Japan.

Copyright 2000 by the American Geophysical Union.

Paper number 2000JD900228.
0148-0227/00/2000JD900228$09.00

[e.g., *Iwasaka et al.*, 1985; *Poole and McCormick*, 1988; *Browell et al.*, 1990; *Stefanutti et al.*, 1995], and with in situ instruments [e.g., *Dye et al.*, 1992; *Deshler et al.*, 1994]. Of these instrument platforms, spaceborne sensors have the advantage of being able to monitor the frequency of PSCs on a large spatial coverage. The Stratospheric Aerosol Measurement (SAM) II sensor on board the NIMBUS 7 spacecraft monitored PSCs continuously over both polar regions since 1978 until January 1994 [e.g., *McCormick et al.*, 1982; *McCormick and Wang*, 1993]. After SAM II ceased operating, the Polar Ozone and Aerosol Measurement (POAM) II instrument took over the observation of PSCs in September 1993. Unfortunately, POAM II stopped in November 1996, when the Systeme Pour l'Observation de la Terre (SPOT) spacecraft was lost [*Fromm et al.*, 1997]. Some sensors on board the Upper Atmosphere Research Satellite (UARS), including the Cryogenic Limb Array Etalon Spectrometer (CLAES) [*Roche et al.*, 1994; *Ricard et al.*, 1995; *Massie et al.*, 1996], the Improved Stratospheric and Mesospheric Sounder (ISAMS) [*Taylor et al.*, 1994], and the Halogen Occultation Experiment (HALOE) [*Hervig et al.*, 1997], can observe PSCs. Unfortunately, the ISAMS failed in 1992, and CLAES ceased to operate in 1993. HALOE is still operating, but it has limited latitude coverage, preventing it from measuring the northern polar winter.

The Improved Limb Atmospheric Spectrometer (ILAS) was launched on board the Advanced Earth Observing Satellite (ADEOS) in August 1996 and started regular operation in November 1996 [*Sasano et al.*, 1995, 1999a,b]. ILAS is an occultation sensor, designed to monitor ozone (O_3) and ozone-related species, such as aerosols (or PSCs), nitric acid (HNO_3), nitrogen dioxide (NO_2), nitrous oxide (N_2O), methane (CH_4), and water vapor (H_2O) at 1-km height intervals [*Yokota et al.*, 1998]. The Sun-synchronous polar orbit of ADEOS and the solar occultation technique used by ILAS made it possible to monitor the polar region on a regular basis, as with SAM II and POAM II. ILAS observed 14 circumpolar points in each hemisphere every day at high latitudes (57.1°-72.7°N and 64.3°-88.2°S). The upper latitude limit varied seasonally [see *Sasano et al.*, 1999a, Figure 1]. ILAS started collecting data in November 1996 and continued until June 1997, when the ADEOS ceased operating because of solar battery failure. It was the only spaceborne sensor that could monitor Arctic PSCs on a regular basis during the 1996/1997 winter. Since ILAS observed a similar range of latitudes as SAM II and POAM II, its data are comparable to those of the previous sensors. The PSC data presented in this paper therefore fill a gap in the long-term PSC monitoring record.

The Northern Hemisphere winter of 1996/1997 was especially important because significant ozone loss was observed over the Arctic. The Total Ozone Mapping Spectrometer (TOMS) on board ADEOS and the Earth Probe satellite observed a record low level of total ozone over the Arctic in late March and early April 1997 [*Newman et al.*, 1997]. A temperature analysis by *Coy et al.* [1997] detected a minimum temperature on the 475 K isentropic surface in the early spring of 1997 that was well below the climatological range of the past 17 years. In winter 1996/1997 the ozone loss over the Arctic was connected to a prolonged polar vortex and the persistence of low temperatures into early spring. ILAS successfully observed the profiles of Arctic ozone and related species at around 65°N throughout winter and spring 1996/1997.

This paper reports the analysis of PSC observations made with ILAS during the winter and early spring of 1996/1997 over the Arctic. This study provides an additional data set for the long-term PSC data archive to examine the long-term trend in PSC frequency. The analysis of ILAS ozone data by *Sasano et al.* [2000] indicated that the local maximum rate of ozone loss was found on the 450 K surface in the latter half of February and amounted to 84 ± 17 ppbv/day. Significant ozone loss rates appear to be well correlated with the PSC occurrences reported in this paper, suggesting a link between heterogeneous reactions on the PSC surfaces and ozone loss. This paper forms a basis for future studies of the mechanism of ozone destruction, including detailed analysis of other minor species.

2. ILAS Instrument and Aerosol Retrieval Algorithm

ILAS has two spectrometers: a 44-channel infrared (IR) spectrometer, operating from 6.21 to 11.76 microns (850-1610 cm-1), and a 1024-channel near-visible spectrometer that operates at wavelengths from 753 to 784 nm (hereafter referred to as the visible spectrometer) [*Sasano et al.*, 1995; *Suzuki et al.*, 1995; *Sasano et al.*, 1999b]. The main measurements made with ILAS are vertical profiles of ozone (O_3) and ozone-related species, all of which can be derived from the infrared transmission spectra at 1-km height intervals. The absorption spectra of oxygen molecules (the O_2 A band) are measured with the visible spectrometer, which provides temperature and pressure profiles, as well as the aerosol extinction at about 780 nm, where absorption by molecular oxygen is negligible.

The ILAS data processing algorithm 4.20 is described in the appendix in detail. Here we only briefly describe how version 4.20 of the algorithm derives the aerosol extinction at 780 nm. Figure 1 depicts schematically a spectrum of pseudo-transmittance at 20 km as an example. Outside the O_2 A band region in the visible spectrometer data, the transmittance consists of contributions of the ozone continuum absorption known as the Wulf band, scattering by air molecules, and scattering/absorption by aerosols. After subtracting the contribution from ozone, determined by functional form fitting, and that of air, calculated using the temperature and pressure data, the remaining attenuation of the solar signal can be attributed to aerosols.

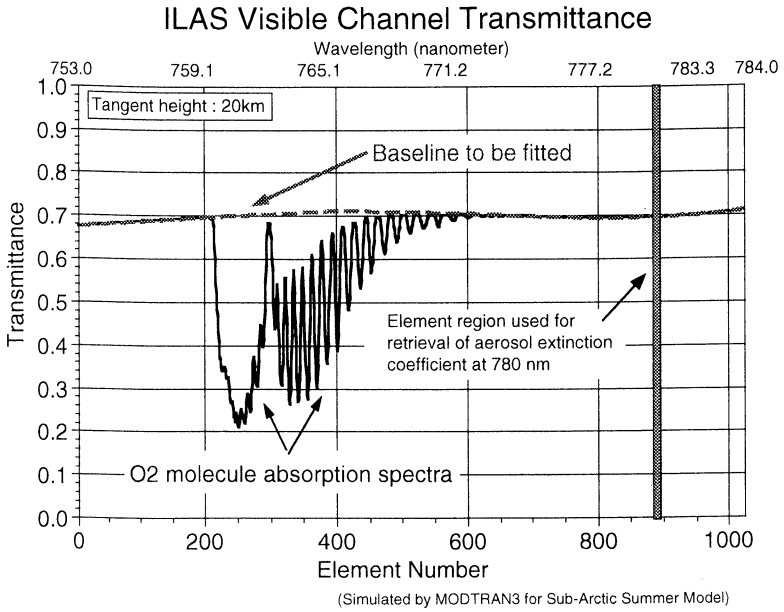

Figure 1. Schematic spectrum of pseudo-transmittance at 20 km observed with ILAS visible spectrometer. The spectrum consists of an absorption due to oxygen A band. See the appendix for the details.

The derived aerosol transmittance as a function of altitude is solved for the extinction coefficient profile at 780 nm. No a priori profile is used in the ILAS data retrieval except for the initial profile, while the retrieved profile does not depend on the initial one. Aerosol extinction coefficients at 1-km intervals in tangent height are regarded as unknowns and retrieved to obtain an aerosol profile. The details of the effective vertical resolutions in consideration of the size of the instantaneous field of view (IFOV) and smoothing process are described in the appendix. The horizontal resolution of an occultation sensor along a line of sight is inherently about 200-250 km at an altitude of approximately 20 km.

Version 4.20 of the algorithm uses the United Kingdom Meteorological Office (UKMO) stratospheric assimilation data [*Swinbank and O'Neill*, 1994] to estimate the Rayleigh scattering, rather than deriving it from the pressure and temperature deduced from the ILAS data, because the determination of these quantities is still being validated. The UKMO stratospheric assimilation data are released daily (at noon UT) for a grid size of 2.5° in latitude and 3.75° in longitude. The ILAS Data Handling Facility (DHF) collocates temperatures and pressures to ILAS measurements on the same day and archives them with the ILAS data. This study uses the collocated temperature and pressure data for comparison with ILAS data and for meteorological analysis.

3. ILAS Data Version 4.20

Figure 2a shows an example of the extinction profiles at 780 nm observed with ILAS over the Northern Hemisphere on June 18, 1997, with the error bars estimated

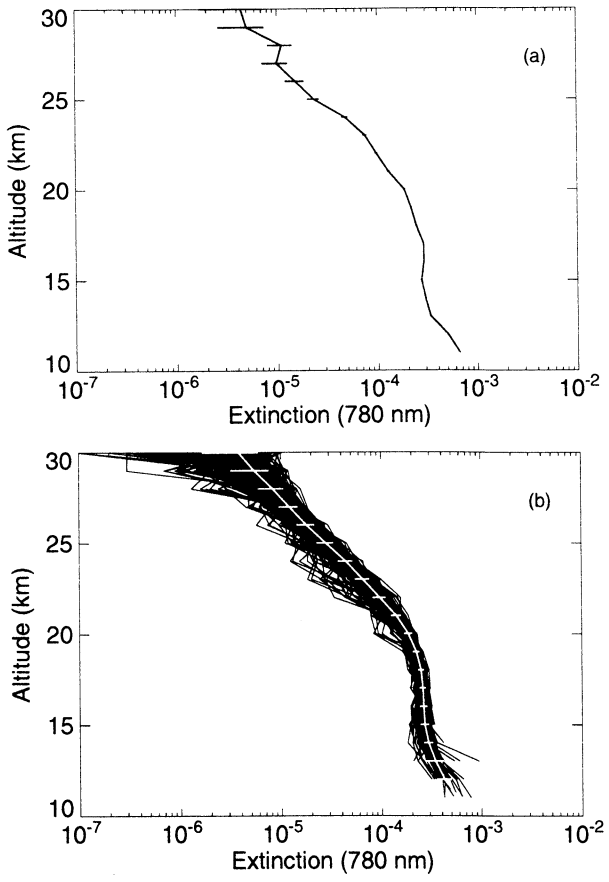

Figure 2. (a) An example of the extinction profiles at 780 nm observed with ILAS over the Northern Hemisphere on June 18, 1997, with the error bars estimated in the version 4.20 algorithm. The error bars ≤ 3, lower altitudes are invisible on the scale used here. (b) All extinction profiles obtained in June 1997 also over the Northern Hemisphere. White lines show the mean and the range of the standard deviation for the data.

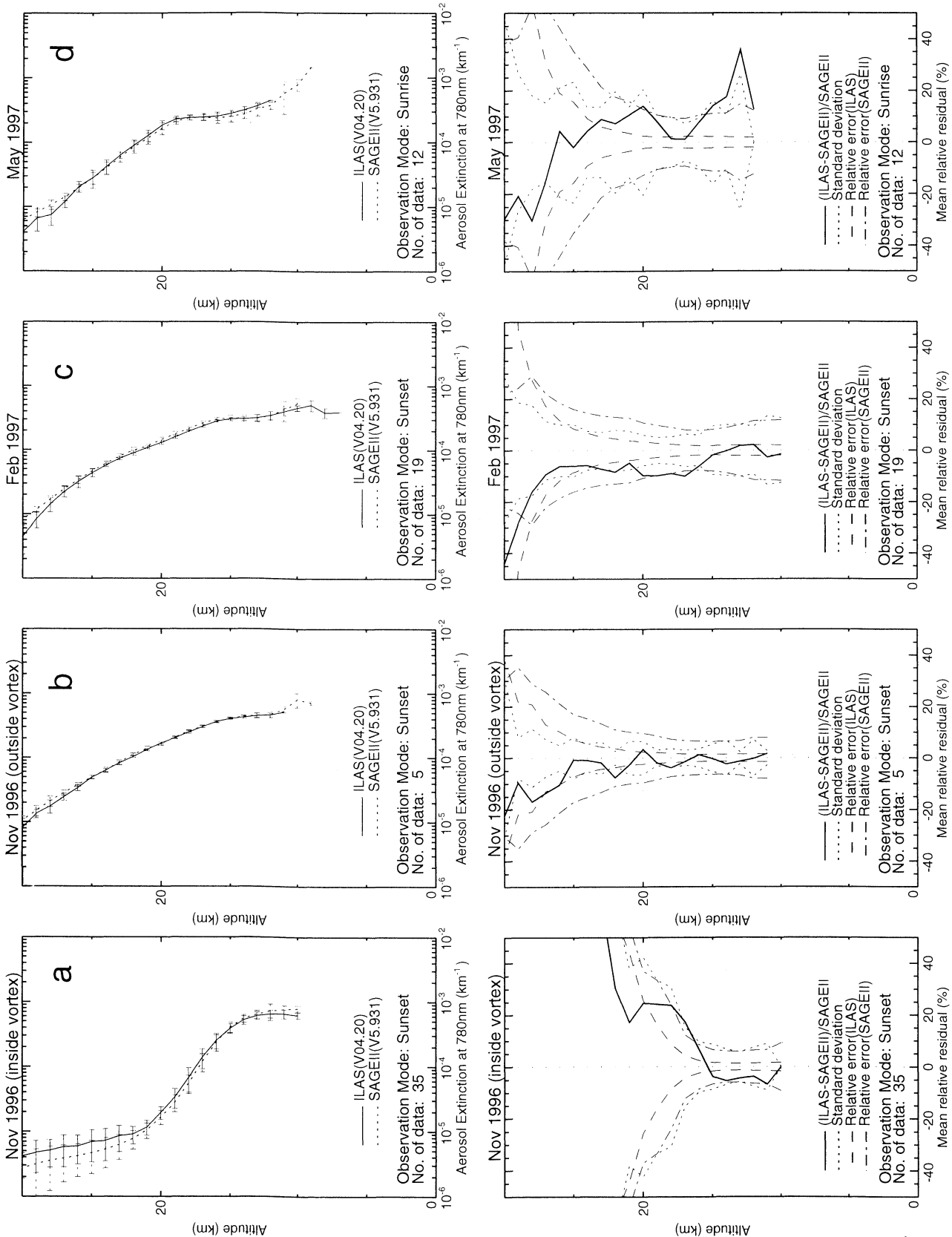
a
b
c
d
Nov 1996 (inside vortex)
Nov 1996 (outside vortex)
Feb 1997
May 1997
Altitude (km)
Aerosol Extinction at 780nm (km^{-1})
ILAS(V04.20)
SAGEII(V5.931)
Observation Mode: Sunset
No. of data: 35
Observation Mode: Sunset
No. of data: 5
Observation Mode: Sunset
No. of data: 19
Observation Mode: Sunrise
No. of data: 12
(ILAS-SAGEII)/SAGEII
Standard deviation
Relative error(ILAS)
Relative error(SAGEII)
Mean relative residual (%)

in the version 4.20 algorithm. Contributing sources of error are considered to be the followings: (1) the error in regression line fitting used to determine the 100% solar signal level, (2) the uncertainty of the Rayleigh scattering contribution, and (3) the uncertainty of the ozone contribution at the Wulf band (see the appendix). All these sources of error are included in the error provided in the version 4.20 data files. Both the random error in the signals and the uncertainty in determining the 100% regression level are of the order of 1.0×10^{-5} km^{-1} and change only a little with altitude between 10 and 30 km. The uncertainty in the extinction coefficient due to Rayleigh scattering is estimated to be of the order of 1.0×10^{-6} km^{-1} at about 25 km and reaches 1.0×10^{-5} km^{-1} at about 11 km, when the temperature uncertainty is assumed to be about 4°. The relative error increases at altitudes above 30 km because the extinction coefficient decreases to 1.0×10^{-5} km^{-1} or less.

Figure 2b shows all of 354 profiles obtained in June 1997 also over the Northern Hemisphere. Mean and the range of the standard deviation for the month data are also indicated. As shown in Figure 2b, there was relatively small fluctuation in the extinction coefficient in summer, demonstrating the reliability of the measurements. The relative fluctuation ratio, determined as the ratio of the standard deviation for the data for 1 month to the monthly mean value at 16 km, was 11% in May and 9.3% in June. These values can be regarded as the upper limit of the random error when atmospheric conditions are stable. They are consistent with the estimated value described above.

Burton et al. [1999] compared 73 pairs of nearly coincident profiles of aerosol extinction observed over the Southern Hemisphere with ILAS version 3.10 and Stratospheric Aerosol and Gas Experiment (SAGE) II version 5.931 for 1 week in January and February 1997. The profiles agree within 10% for altitudes from approximately 15 to 24 km, although there was a small systematic bias for the upper altitudes.

ILAS version 4.20 of the algorithm includes the correction for the solar limb darkening effect (see the appendix), which biased the aerosol extinction profiles in the previous versions. The correction for the effect in terms of the extinction coefficient is about 3×10^{-5} km^{-1} at an altitude of 20 km, and decreases with altitude. To see the effects of the corrections and modifications in the version 4.20 algorithm, Figure 3 compares SAGE II and ILAS version 4.20 for 40 profiles in November 1996, and 19 profiles in February 1997 over the Southern Hemisphere, and for 12 profiles in May 1997 over the Northern Hemisphere. The November data are separated into two groups, one containing profiles inside the polar vortex (35 profiles) and the other containing profiles outside it (five profiles). The upper panels compare the average profiles for SAGE II and ILAS. The horizontal bars indicate the one-sigma standard deviation of each. The lower panels depict the mean fractional differences between the ILAS and SAGE II data (solid curve), the root-mean-square of the fractional differences (dotted curve), and the ILAS (dashed curve) and SAGE II measurement errors (dashed and dotted curve). The mean fractional differences are within the uncertainties of the ILAS and SAGE II measurement errors and are in the range of 10-20%. The agreement in November 1996 appears poorer for inside the vortex than for outside the vortex, but this is because the extinction values are as low as 1.0×10^{-5} km^{-1} at above 20 km. The ILAS profiles in version 4.20 are considerably improved over version 3.10 and show very good agreement with the SAGE II profiles. This comparison demonstrates that the ILAS version 4.20 aerosol data are valid for scientific use. ILAS version 4.20 data are released for registered users, and version 3.10 data of ozone, nitric acid, and aerosols are open for all users on ILAS homepage at http://www-ilas.nies.go.jp/.

4. Identification of PSCs

Poole and Pitts [1994] reported the climatology of PSCs based on the SAM II long-term data archive. In their approach all the extinction data inside the polar vortex were averaged for each altitude level and for each 10-day period where the collocated temperature was above 200 K. The threshold value used to identify PSCs was determined as the median plus 3 times the median deviation. All extinction values larger than the threshold were identified as PSCs when the collocated

Figure 3. Comparisons of the extinction coefficients at 780 nm using ILAS version 4.20 and SAGE version 5.931. The top panels compare the monthly average profiles. The 40 profiles observed in November 1996 were divided into two groups, depending on whether they were inside or outside the polar vortex. From the left, comparisons of (a) 35 profiles over the Southern Hemisphere in November 1996 inside the vortex, (b) 5 profiles outside the vortex the same month, (c) 19 profiles over the Southern Hemisphere in February 1997, and (d) 12 profiles over the Northern Hemisphere in May. The bottom panels depict the mean fractional differences between the ILAS and SAGE II data (solid curve), the root-mean-square of fractional differences (dotted curve), the ILAS measurement error (dashed curve), and the SAGE II measurement error (dashed and dotted curve). The SAGE II extinction coefficients at 525 and 1020 nm were converted to 780 nm by interpolating the logarithms of the extinction coefficients. Note that *Burton et al.* [1999] applied the method of *Thomason* [1991] for interpolation, but the difference between the conversion methods is not significant.

temperature was lower than 200 K. *Fromm et al.* [1997] adopted a similar method, but they selected "clear-sky" profiles prior to the analysis, rather than selecting background profiles from warm areas. They determined the threshold value as the mean of the clear-sky extinction values plus 4 times the standard deviation, without specifying T <200 K.

To identify PSC events, we adopted an approach similar to those of *Poole and Pitts* [1994] and *Fromm et al.* [1997]. First of all, the definition of *Nash et al.* [1996] was applied to determine the vortex boundary (M. Ninomiya and H. Nakane, private communication, 1999) using the UKMO stratospheric assimilation data. Then the ILAS data were divided into two groups, corresponding to inside and outside the polar vortex.

As ILAS measured 14 circumpolar points at almost the same latitude (64°- 70°N) every day, a maximum of 140 events could be obtained in each 10-day period. In actuality, some events are lost due to trouble with telemetry data acquisition and significant electric noise, and therefore data for about 110-140 events are available for each 10-day period. Figure 4 shows the contour for the number of events for which ILAS data were obtained inside the vortex (N_{in}) and used for our analysis. For example, 84 events were obtained for inside the vortex during the first 10-day period in February at a 20-km altitude, while the total of the ILAS measurements at the period (not shown in the figure) was 131. The blank area in Figure 4 indicates that no ILAS data were obtained inside the vortex ($N_{in} = 0$). As the polar vortex is formed from higher altitudes to lower altitudes, the height range of the polar vortex at the latitude of the ILAS measurement varies with time. In the beginning of the formation of polar vortex in December 1996 and January 1997, ILAS could look at inside the vortex only at higher altitudes (for example, above 20-km altitude at the beginning of January). As stated above, we determined the polar vortex boundary at each altitude level and analyzed only the data inside the vortex (see Figure 4). As many of the PSC profiles were obtained near the boundary region of the polar vortex in January, some PSC events at lower altitude could be excluded because they were outside the vortex though near the edge, but our careful examinations showed those events are very few.

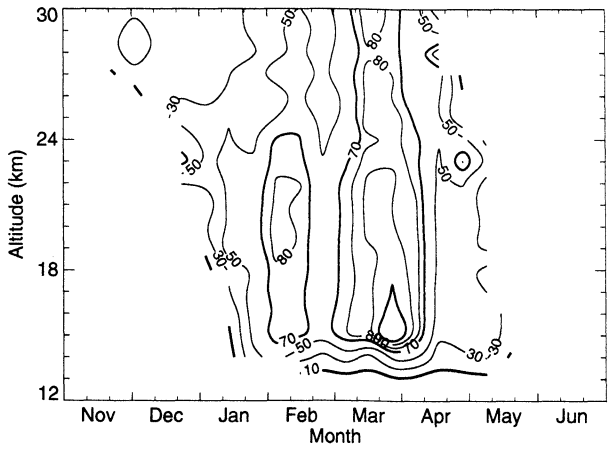

Figure 4. The contour for the number of measurements for which ILAS observed inside the vortex (N_{in}) and used for the analysis. The blank area indicates that no ILAS data were obtained inside the vortex. As the polar vortex is formed from higher altitudes to lower altitudes, the height range of the polar vortex at the latitude of the ILAS measurement varies with time. The latitudes of ILAS measurements are shown by *Sasano et al.* [1999a, Figure1]. See text for the details.

The polar vortex is not usually situated symmetrically with respect to the polar axis, and its boundary is near the same latitudes at which the ILAS measurements were made. Therefore the ILAS would observe inside the vortex several times in a row and then several times outside the vortex, and this pattern would be repeated. Therefore the statistical analysis discussed in this paper is neither the average nor representative for all the polar vortex area. This is an inherent disadvantage of the occultation method. Figure 4 shows where ILAS observed and complements the information needed to interpret the following figures.

All the extinction data inside the polar vortex were averaged for each altitude interval and for each 10-day period when the collocated temperature was above 200 K, as adopted by *Poole and Pitts* [1994]. To determine the threshold value, histograms of the frequency of measurements for the extinction values were scrutinized carefully, and the mean plus 5 times the standard deviation was adopted as the threshold. No temperature criterion (T <200 K) was included in the identification, as in *Fromm et al.* [1997], in part because of the uncertainty in the UKMO stratospheric temperature. *Pullen and Jones* [1997] showed that the UKMO temperature has a positive bias of 1.7° at around the temperature of nitric acid trihydrate (NAT) formation. A temperature criterion was also eliminated because temperature history is more important for PSC formation than collocated temperatures [*Stefanutti et al.*, 1995; *Larsen et al.*, 1997].

Figure 5 shows the time variation of the threshold values (thick lines) at 23 km adopted in this analysis, along with the mean values (thin lines) of the extinction coefficient where T >200 K. It is well known that the background aerosol level is much lower inside the vortex than outside [e.g., *Thomason and Poole*, 1993]. Therefore, with the beginning of the formation of the polar vortex in December and January, the threshold value decreased considerably with time. Most of the ILAS measurements in mid-January are from cold areas, and there were less than 10 cases in which the background aerosol condition (T >200 K) was observed at 21-28 km altitudes inside the vortex. For this period it is rather difficult to determine the threshold statistically. In our analysis we first determined the threshold for this period in the same manner as for the other periods (thick solid line). Then we also examined the other threshold

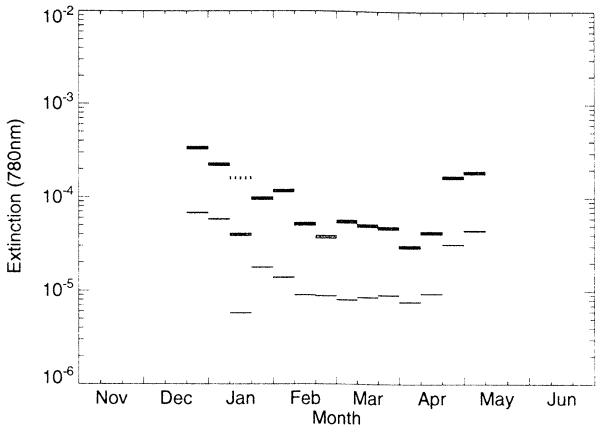

Figure 5. The threshold values for PSC identification at an altitude of 23 km. The threshold values (thick lines) were determined as the mean value (thin lines) plus 5 times the standard deviation for the background aerosol data that are corresponding to warm (T >200 K) area (threshold 1). They were determined for each 10-day period and for each 1-km altitude interval and time varying. The thick dotted line in mid-January shows the other threshold (threshold 2) determined by interpolating the values for before (first term of January) and after (last term of January) the period.

that is an interpolated value before and after the period (thick dotted line), although there is a large temporal variation during the period. We return to the effects of threshold determination on PSC identification later.

We applied these criteria to all the extinction data and selected the values exceeding these criteria. The data with a relative error exceeding 100% (mainly above an altitude of ~27 km) were eliminated. We did not introduce the High Z_{min} PSC criterion applied by *Fromm et al.* [1997] because PSCs observed over the Arctic are optically thin enough to ensure that most profiles can be successfully extended to a lower altitude without truncating the signal. Some of the PSCs observed by the ILAS over Antarctica in June 1997 appeared truncated at lower levels. The high Z_{min} PSC criterion should possibly be included in the analysis of Antarctic PSCs, but it appears to be unnecessary for Arctic PSCs.

Using these criteria, PSC profiles that include a "5-sigma selected" value for at least one altitude were chosen. Figure 6 shows typical PSC profiles observed in January (Figure 6a), February (Figure 6b), and March (Figure 6c) inside the vortex. The 5-sigma selected values are marked with circles. Most of the thick, dense PSC profiles were observed in mid-January, while the PSC profiles observed in February and March were thinner and less intense. Each PSC profile was compared with the corresponding UKMO temperature profile in Figure 6, and good consistency was found between the enhancement of the extinction coefficient and low temperature.

Most of the PSC profiles look like those in Figure 6, but some of the selected profiles do not have a very sharp layered structure like them. We sometimes found that the histogram of the frequencies of extinction coefficients for each 10-day period and each altitude has a continuous feature between the background mode and PSC mode. We tried to determine the threshold of PSC identification in several ways, using different multiples of the standard deviation. No matter how the threshold is determined, an ambiguous part in the extinction

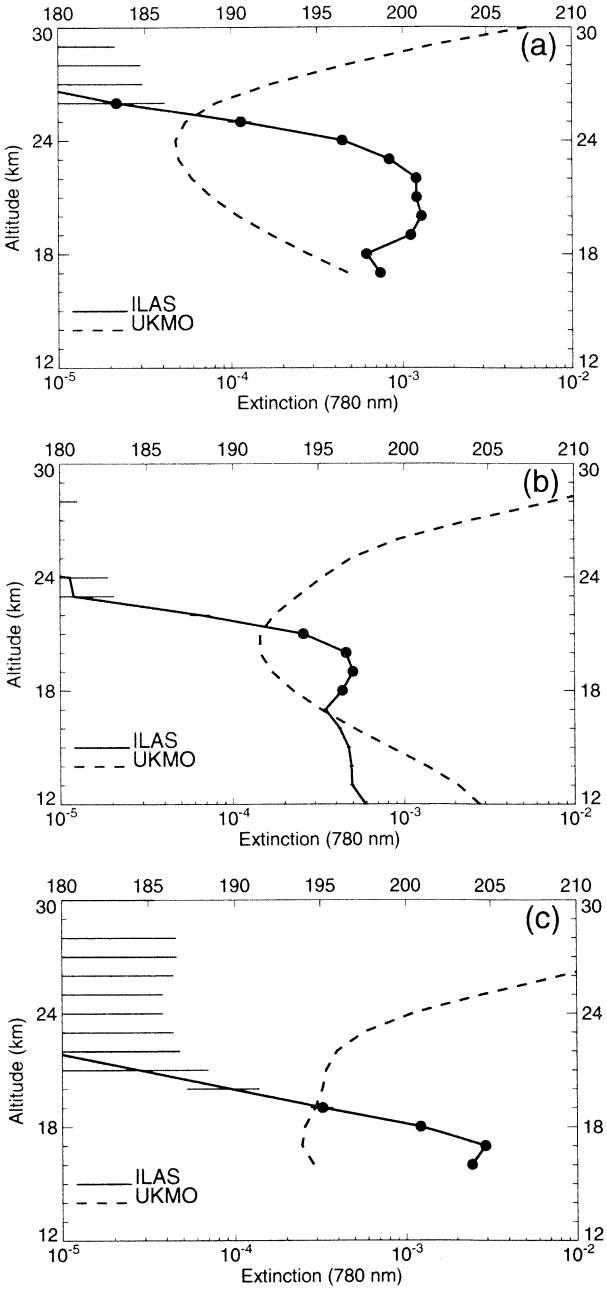

Figure 6. Typical PSC extinction profiles observed with the ILAS over the Arctic on (a) January 20, (b) February 24, and (c) March 10 1997, with error bars (invisible for some points). The collocated UKMO temperature profiles are shown as dashed lines (top scale). The "5-sigma selected" values are marked with circles. Good consistency is seen between the enhancement of the extinction coefficient and low temperature.

range remains near the threshold value. Actually, the ILAS aerosol extinction values are the average for the entire sampling volume, which covers about 230 km (at an altitude of approximately 20 km) in the direction of the field of view, although the field of view is only 2 × 2 km. As discussed by *Hervig et al.* [1997], a PSC could have spatial dimensions smaller than the sampling volume of an occultation sensor, and degradation of the actual PSC extinction can occur when the cloud is distributed nonuniformly in the sampling volume. This is an additional inherent limitation of an occultation sensor. The critical values that are close to the threshold should be examined carefully to judge whether they are really PSCs. T_{NAT} is one of the references to validate PSC identification. We compare the 5-sigma selected data with the NAT formation temperature in the following section.

5. Comparison With the NAT Formation Temperature

The ILAS collocated temperatures were compared with the NAT formation temperature T_{NAT} calculated using the formula of *Hanson and Mauersberger* [1988], as a function of the mixing ratios of nitric acid and water vapor. To estimate T_{NAT} accurately, we used the available ILAS nitric acid and water vapor data as well as aerosol data. The version 3.10 ILAS nitric acid data were validated by *Koike et al.* [2000], demonstrating the reliability of the data. The ILAS Science Team members are still doing a validation analysis of the water vapor data derived with the ILAS, but preliminary comparisons show that the version 4.20 water vapor data agree well with independent validation data (H. Kanzawa and Laura Pan, private communication, 2000).

In the case of a PSC sighting, the PSC absorption spectra might affect the gas absorption spectra, sometimes resulting in a large bias in the gas-mixing ratio. In an algorithm test, simulation showed that the effect of PSCs on nitric acid is negligible because nitric acid molecules have a strong absorption band in a spectral region that is almost free from PSC absorption spectra. On the other hand, the effect of PSCs on retrieval of water vapor is more significant. The effects of PSCs on the gas species at 22 km are estimated to be about -0.2 to +0.9 ppbv for nitric acid, while they are roughly -5.7 to -0.03 ppmv for water vapor. However, the accuracy for background aerosols is much better than for these gas species.

Table 1 summarizes the conditions used to estimate the NAT temperature. For reference, the fixed (climatological) values used for the mixing ratio of nitric acid and water vapor were 9 ppbv and 5.5 ppmv, respectively (case 1 in Table 1). In case 2 we estimated the background levels of nitric acid and water vapor for each 10-day period from the average of the data corresponding to background aerosols, where the collocated temperature was warm enough (T >200 K). This background estimate should avoid the effect of PSC disturbance on the water vapor data. The correlation with T_{NAT} for cases 1 and 2 was closely examined, and it was found T_{NAT} is essentially the same in both cases at an altitude of 20 km. Since the mixing ratio of water vapor and nitric acid depends on altitude, there is a slight shift in T_{NAT} (case 2) from the reference T_{NAT} (case 1) at other altitudes, but the difference is less than 1°. Although validation studies for the water vapor data for ILAS version 4.20 are incomplete, this result suggests that the ILAS 4.20 water vapor estimates are stable according to the background aerosols and can provide a reasonable estimate of T_{NAT}.

Figure 7 is a scatterplot of the extinction versus temperature difference between the collocated temperature and the estimated T_{NAT} for case 2 in mid-January. Case 1 is not illustrated, but the results are so similar that the difference is indistinguishable on the scale used here. The solid circles in Figure 7 show the extinction values that are larger than the mean plus five standard deviations. The different panels in the figure show the results for each different altitude obtained using different threshold values (see Figure 5).

As already pointed out above, the threshold value at 21-28 km in mid-January, when enhanced extinction was frequently observed, was determined using less than 10 sampling points because there was a lack of data for warm areas. We repeated the analysis with another threshold by interpolating before and after the period. The threshold determined as the mean plus five standard deviations (solid lines in Figures 7a-7f)

Table 1. Summary of the Condition for T_{NAT} Estimation

	Nitric Acid	Water Vapor
Case 1	9 ppbv	5.5 ppmv
Case 2	background value*	background value*
Case 3	ILAS collocated	background value*

*Background values are determined as the average of data that correspond to the background aerosols where the collocated temperature is warm (T >200 K).

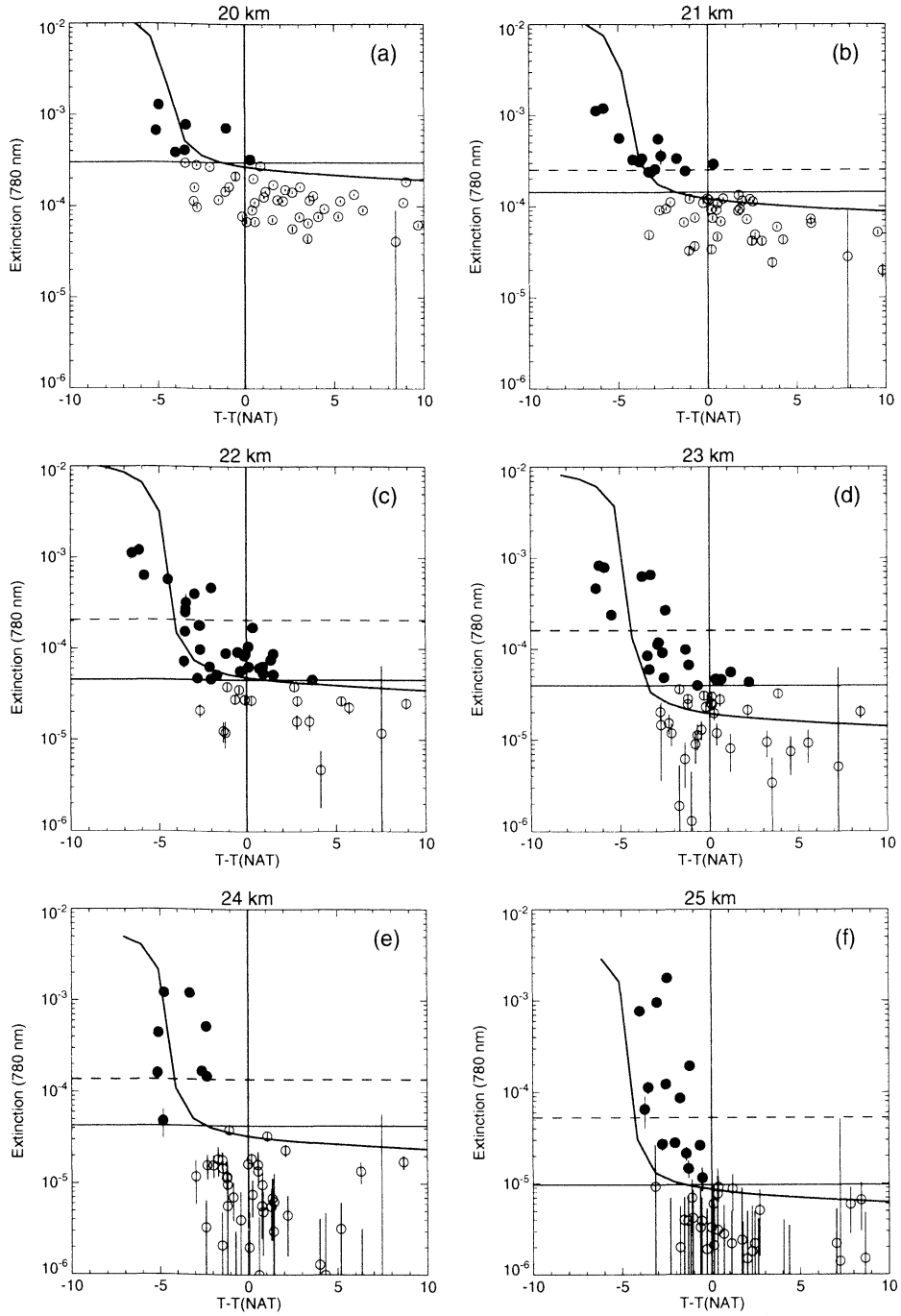

Figure 7. Scatterplot of the ILAS extinction coefficient versus the temperature difference between the collocated and NAT temperatures for case 2 (see Table 1) for mid-January 1997 at each altitude level from 20 to 25 km. (a-f) The solid line indicates threshold 1 determined as the mean plus five standard deviations, and (b-f) the dashed line shows threshold 2, determined by interpolation of the values for just before and after the period. Solid circles show extinction coefficients above threshold 1 ("5-sigma-selected" values: see text for the details). Error bars are shown with the extinction values, although they are not distinguishable on a figure of this scale for large extinction values. In the figure, the particle formation curve for supercooled ternary solution (STS) is also indicated. This curve was calculated by using the thermodynamic model developed by *Carslaw et al.* [1995].

looks somewhat low because some PSC-values are less than $\sim 10^{-4}$ at a temperature warmer than T_{NAT}. The other threshold interpolated before and after the period (dashed lines in Figures 7b-7f) seems a little too high, although beyond which all data are found at a temperature lower than T_{NAT}. Some events whose extinction coefficients are smaller than the latter threshold (dashed line) really look like PSC events because their

profiles show clear layered structure and/or are found at 3°~ 4° below T_{NAT} (see Figures 7c and 7d). For those ambiguous events we need further investigation one by one. Although there is uncertainty in threshold determination, it is clear in Figure 7 that all of the extremely high extinction coefficients with values larger than about 2×10^{-4} km^{-1} are found at temperatures several degrees lower than T_{NAT}, suggesting formation of particles of supercooled ternary solution [*Carslaw et al.*, 1994; *Tabazadeh et al.*, 1994, 1995; *Larsen et al.*, 1997].

In Figure 7 the particle formation curve for supercooled ternary solution (STS) was also indicated. This curve was calculated by using the thermodynamic model developed by *Carslaw et al.* [1995]. The amount of sulfate was taken to fit the background aerosol profiles observed with ILAS. Mie theory was applied to convert the ILAS 780-nm extinction into volume, based on some measurements of size distribution, using a refractive index that depends on temperature [*Luo et al.*, 1996; *Beyerle et al.*, 1997]. Nitric acid and water vapor data were taken from the background average as for the NAT formation temperature. Comparing the extinction data with the thermodynamic equilibrium curve of STS particle formation in Figure 7, the events with extremely high extinction coefficients are consistent with STS formation. However, some PSC data (black dots) at around T_{NAT} do not seem to follow the curve, suggesting other types of PSCs though we need more careful investigations for them.

Since the accuracy of the nitric acid data is thought to be adequate, even for the case of the PSC described above, T_{NAT} was again estimated using collocated ILAS nitric acid data (see case 3 in Table 1). On the other hand, some of the nitric acid profiles that correspond to large PSC events are quite low, which implies that nitric acid is being removed from the gas phase by particles. Figure 8 shows an example of a decrease in the nitric acid data that corresponds to enhanced aerosol extinction. In such cases the background nitric acid value should be used to estimate T_{NAT}, rather than the collocated value, because the particles should have formed before the nitric acid decreased.

The comparison of T_{NAT} for cases 2 and 3 shows that the difference is not significant for small extinction coefficients ($<1.0 \times 10^{-4}$ km^{-1}), while in case 3 T_{NAT} is much lower for large extinction coefficients ($>2.0 \times 10^{-4}$ km^{-1}). This is due to the decrease in nitric acid, as shown in Figure 8. There is a negative correlation between nitric acid and the aerosol amount, which is still under investigation, and the details are beyond the scope of this paper.

Since the UKMO data are provided daily (at noon), the time difference between the collocated and UKMO temperatures is up to 12 hours. To examine the effect of the time difference on the collocated temperature used in the analysis above, we estimated the exact temperature at the time of the ILAS measurements by interpolating from the original temperature data, but did not find any significant difference between the original and interpolated temperatures. The inherent uncertainty of the UKMO temperature is more significant. *Pullen and Jones* [1997] reported that the UKMO temperature includes a positive 1.7 K bias and about 2 K of random

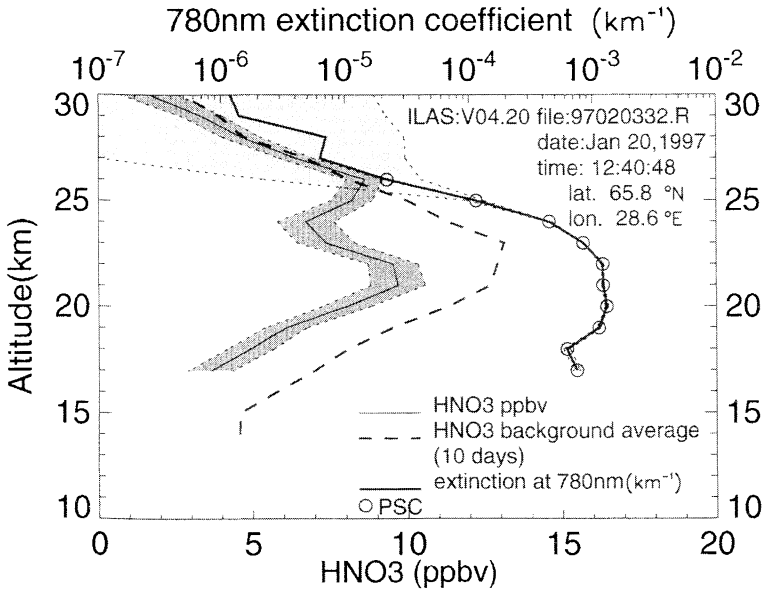

Figure 8. The nitric acid profile observed on January 20, 1997, at 65.8°N, 28.6°E (thin solid line, bottom scale). The dashed line shows the background profile of nitric acid for the 10-day period in mid-January 1997. The thick solid line shows the aerosol extinction profile observed at the same time (top scale). The 5-sigma-selected PSC values are shown with circles. The shaded areas show the range of errors.

scatter at the NAT point temperature. This temperature overestimation might affect our analysis.

After these careful examinations, we concluded that considerable number of the 5-sigma-selected data correspond to temperatures lower than T_{NAT}; therefore the criteria used to select PSC data were quite reasonable. However, some PSC values (solid circles in Figure 7) were still found at temperatures above T_{NAT}. Recent studies by *Tabazadeh et al.* [1995] and *Larsen et al.* [1997] demonstrated the importance of temperature history rather than the temperature collocated with the PSC event. *Stefanutti et al.* [1995] observed "warm" PSCs over Antarctica with lidar. Therefore we cannot refute the existence of warm PSCs. Since the degradation of extinction coefficients may cause ambiguity in PSC identification, those warm PSCs should be examined carefully. We are now conducting intensive trajectory analysis and investigating the potential vorticity of the warm PSCs, and the results will be reported in our next paper. Here we call the 5-sigma-selected values found at temperatures lower than T_{NAT} the T_{NAT}-selected values, and discuss them separately in the following section.

6. PSC Locations

Plate 1 shows the PSC locations in the longitude-height cross section for January (Plate 1a), February (Plate 1b), and March (Plate 1c) 1997 along with the lowest temperature collocated to the ILAS measurements. In the Plate, the T_{NAT}-selected values are shown by red dots. The ILAS latitudinal variation was 64°-68°N in January, 68°-70°N in February, and 70°-69°N in March.

In January and February, most PSCs appeared between 90°E and 90°W, centered on the Greenwich meridian, while in March the PSCs appeared much farther east, at approximately 120°E, and at lower altitudes. The results for January and February are similar to the 10-year ensemble average of PSC sightings presented by *Poole and Pitts* [1994], who compared the PSC sightings with NOAA zonal mean temperatures and demonstrated that a strong zonal wave number 1 pattern typical of the Arctic winter was evident. Our analysis shows a similar distribution of PSCs in January and February 1997, but also the interesting appearance of PSCs over Siberia in March. The potential vorticity maps for the period show that the polar vortex was dislocated and spread toward Siberia in March.

The results shown in Plate 1 are only one cross section of the picture of PSC appearance over the entire Arctic, and the limited latitudinal coverage of an occultation sensor sometimes underestimates the PSC events [e.g., *Austin et al.*, 1986]. The PSC frequency seen in occultation is the instrument's frequency, not the atmosphere's. Nevertheless, occultation measurements are valuable because limb-viewing sensors have much lower spatial resolution and ground-based instruments such as a lidar do not have global coverage.

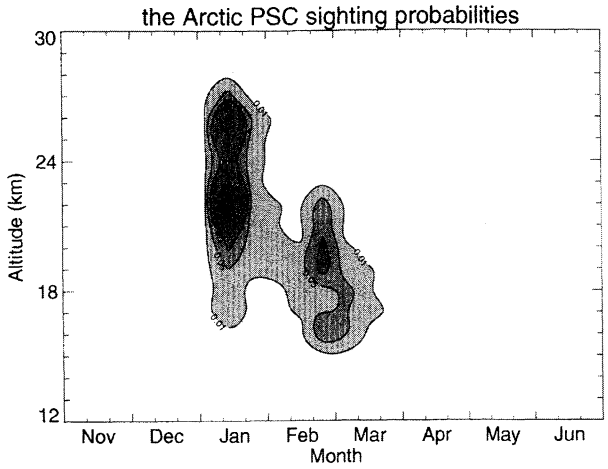

Figure 9. A time-height cross section of the calculated PSC sighting probability (Probability). The PSC sighting probability was defined as the ratio of the number of T_{NAT}-selected PSC events to the number of ILAS measurements inside the vortex (equal to N_{in} as shown in Figure 4) for every altitude and every 10-day period. The product of the number of ILAS measurements inside the vortex shown in Figure 4 and the sighting probability gives the real number of PSC events observed with ILAS for each 10-day period and each 1-km altitude interval. That is (the number of PSC events) = (N_{in}) × (Probability). Contours are shown for 0.01, 0.05, 0.1, 0.3 from outside.

Finally, the PSC sighting probability was calculated as the ratio of the number of PSC events that are T_{NAT}-selected to the number of measurements inside the vortex (as shown in Figure 4) for every altitude and every 10-day period (Figure 9). T_{NAT} selection might underestimate the real PSC sighting probability as it excludes the possibility of warm PSCs, but here we adopted T_{NAT} selection as a precaution. That is, the sighting probability is defined as

$$(probability) = (N_{NAT})/(N_{in}) \quad (1)$$

where N_{NAT} is number of the data of T_{NAT}-selected PSCs. Here we took the denominator of equation (1) as N_{in}, while *Pool and Pitts* [1994] took it as the total number of SAMII measurements including those both inside and outside vortex. This is because ILAS frequently observed boundary region of vortex and the number of inside vortex data varied with time significantly (see Figure 4). The product of the number of ILAS measurements inside the vortex (N_{in}) shown in Figure 4 and the sighting probability (Prob.) gives the real number of PSC events observed with ILAS for each 10-day period and each 1-km altitude interval. That is (the number of PSC events) = (N_{in}) × (Probability).

ILAS observed most frequent PSC events in mid-January, at an approximate altitude of 23 km, and subsequently observed intermittently at approximately 18 km until mid-March. To compare the 1997 results with those of previous years, we analyzed the SAM II data distributed on CD-ROM, following the analysis by

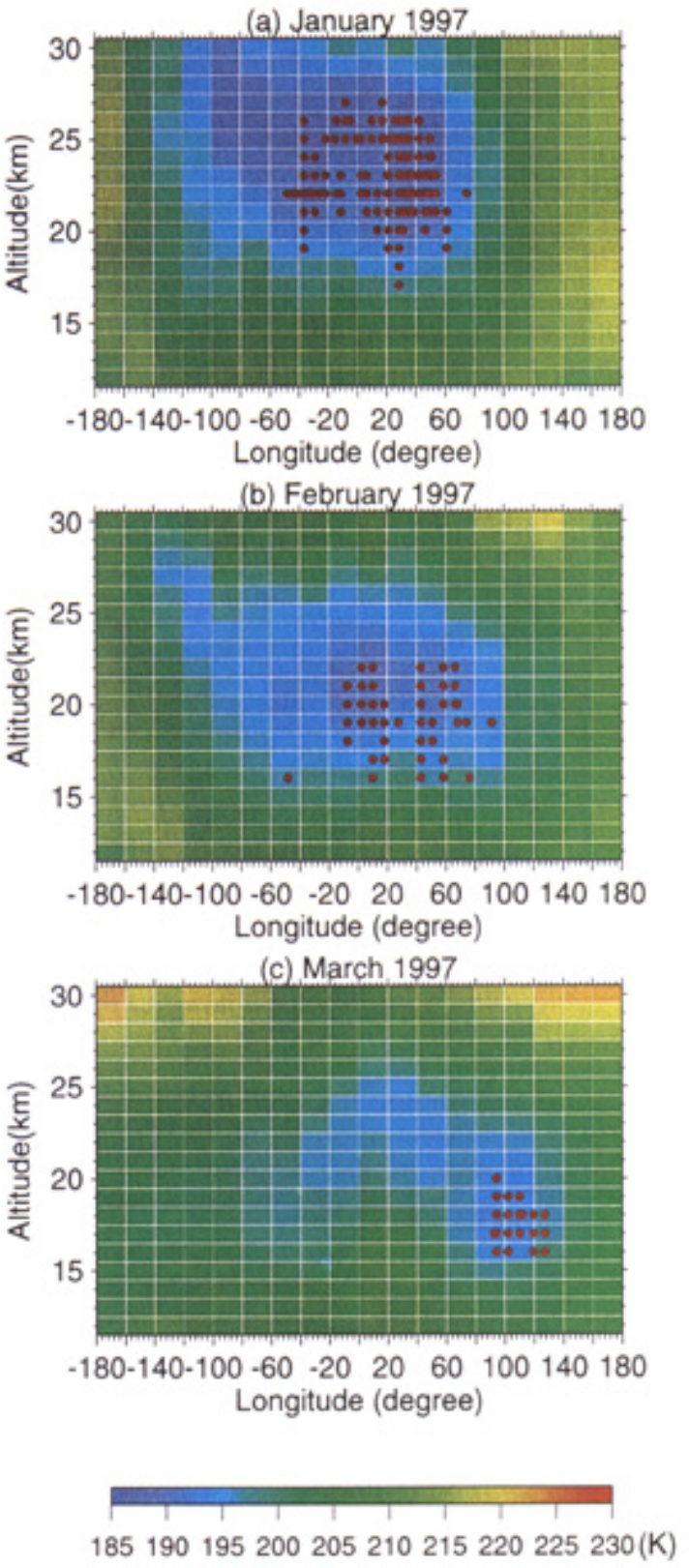

Plate 1. Longitude-height cross section of the PSC events in (a) January, (b) February, and (c) March 1997 along with the lowest temperature collocated to the ILAS measurements each month (color scale for the temperature is shown below the plate). All of the red dots are for T_{NAT}-selected PSC events that correspond to temperatures lower than T_{NAT}.

Poole and Pitts [1994]. The appearance of PSCs until March was observed only in cold winters, such as those of 1980, 1986, and 1988. In these years the winters were long and cold, and no major sudden warming occurred until March, as in 1997. The 1997 Arctic winter was characterized by the prolonged appearance of PSCs until mid-March.

The PSC observations reported in this paper are from a single set of spaceborne measurements made over the Arctic in winter 1996/1997. This PSC data should be added to the long-term PSC data archive. A combined analysis with other gas species observed with ILAS should help to elucidate the mechanism of ozone destruction over the Arctic that winter.

7. Concluding Remarks

The ILAS version 4.20 algorithm provided aerosol extinction data at 780 nm for both polar regions for the period from November 1996 to June 1997. A comparison with the SAGE II data showed good consistency with the ILAS version 4.20 aerosol data at 780 nm, which demonstrated the validity and reliability of the ILAS aerosol data for scientific use. Winter 1996/1997 is well known for its long-lasting polar vortex and significant ozone loss over the Arctic, and the ILAS measurements of aerosols and other gas species were the only spaceborne measurements made on a regular basis (14 times daily) during that period.

The Arctic aerosol data were closely analyzed for winter 1996/1997, when a significant ozone decrease was observed. ILAS observed more than 60 PSC profiles from January through March 1997 over the Arctic, when the threshold of PSC identification was set as the mean plus five standard deviations. In spite of the limitations in determining the threshold, many of the identified PSC events are seen at a temperature below the NAT formation temperature. ILAS observed active PSC occurrence in mid-January at an approximate altitude of 23 km, followed by intermittent occurrence until mid-March, at approximately 18 km. A comparison with past records reveals that it is unusual for PSC events over the Arctic to persist until March.

The aerosol extinction coefficient was clearly enhanced at temperatures several degrees lower than the NAT temperature, which suggests the formation of particles of a supercooled ternary solution though we need further investigation. A significant decrease in the mixing ratio was observed in some nitric acid profiles corresponding to intense PSC events, which suggests the uptake of gas-phase nitric acid into particles.

Appendix

The following describes in detail the algorithm for deriving a profile of the aerosol extinction coefficient at 780 nm. Since ILAS made atmospheric measurements with the solar occultation technique, it is assumed in the data processing that the atmosphere is horizontally homogeneous and has distributions only in the vertical direction. The atmosphere is divided into layers with 1 km thickness between the altitudes of 7 km and 71 km, and the unknowns of aerosol extinction coefficient set at the layer boundaries are solved with an appropriate inversion technique. The lowest layer height varies according to the measurement condition, so that the number of unknowns depends on measurement events.

Aerosol extinction information is derived from visible spectrometer data obtained with 1024 detectors. Its instantaneous field of view (IFOV) has a rectangular shape (1.67 arcmin vertically and 2 arcmin horizontally), which gives a vertical spatial resolution of about 1.6 km at the location of tangent height. While the tangent height varies according to the satellite movement, the ILAS visible spectrometer continuously detects sunlight, and samples its 1024-channel signals in 12 Hz and records them as a time series.

A time series of signals (raw data) with 12 Hz sampling for one solar occultation event contains measurements of deep space for 0% level signals, those of atmospheric transmission of sunlight, and those of exoatmospheric and direct sunlight for 100% level signals, in 11 bits (2048 counts) of resolution. As the first step of data processing, these three data streams are extracted from the raw data and labeled as level 0 data.

A median filter is then applied to the extracted level 0 data to detect and correct abnormal or missing data. If the difference in value between the data of interest and an 18-point average around the data point exceeds a certain criterion, then the filter replaces the data with the median of the 18 points of data. The criterion for atmospheric transmission data is 20 counts, and that for 0% and 100% level data is 5 counts, taking into consideration natural variability. Unfortunately, the filter still has a possibility of mistakenly correcting significant data points (PSCs in our case) by regarding them as noises. To avoid this in the version 4.20 processing, a careful manual check was applied to the cases in which the median filter was operated consecutively for more than one data point, and 18 cases in total were treated without the median filter to generate products.

A pseudo-transmittance spectrum $\tau(t)$ was then calculated from the level 0 atmospheric measurement data for each detector element by the following equation:

$$\tau(t) = \{I(t)\text{-}I_0(t)\}/\{I_{100}(t)\text{-}I_0(t)\},$$

where $I(t)$ is the signal from atmospheric measurement at time t; $I_0(t)$ is the 0% level signal (bias) at time t estimated from a linear interpolation of deep space signals before and after the atmospheric measurements; and $I_{100}(t)$ is the 100% level signals at time t estimated from a linear extrapolation of the exoatmospheric Sun signals. The interpolation and extrapolation of 0% and 100% signal levels for the atmospheric measurement period are done to reduce uncertainties resulting from the

effects of instrument temperature changes. Spectrum $\tau(t)$ is stored as level 1 data for further processing.

An 11-point moving average is applied to level 1 data to reduce random noises. Data sampling is carried out in 12 Hz, but the sampling interval in terms of tangent height varies according to the change of tangent height due to atmospheric refraction. A numerical simulation has shown that the tangent height difference between samplings varies from 0.10 km at 15 km, 0.16 km at 25 km, 0.22 km at 35 km, 0.25 km at 45 km, to 0.26 km at 55 km and above. An 11-point moving average to the data stream is reflected as an 11 × enlargement of sampling height intervals. Thus the effective vertical resolutions with the size of the IFOV taken into consideration are 1.9 km at 15 km, 2.6 km at 25 km, 3.2 km at 35 km, 3.5 km at 45 km, and 3.7 km at 55 km and above.

Tangent height for each datum as a time series in 12 Hz is calculated in the following way. The ILAS instrument employs a "Sun-edge sensor" for geometrically calculating tangent height, which supplies information on angle difference between the top edge of the Sun and the IFOV direction from its 1024 detector array data. This angle data, together with astronomical data on the Sun position and the Earth position, and the satellite position data, are used in version 4.20 data processing to geometrically calculate tangent heights, when atmospheric refraction effects are correctly taken into consideration. The refraction calculation is made at every 5 km along the ray path with the ray trace technique, and also at each atmospheric layer boundary along the path. In this ray trace calculation the shape of the Earth is assumed as a sphere with the local radius at the latitude of the measurement point. Temperature and pressure data supplied from United Kingdom Meteorological Office (UKMO) stratospheric assimilation data [*Swinbank and O'Neill*, 1994] at 1200 UT for each day of ILAS measurement are used for this calculation. Temperature and pressure data for ILAS observation locations (longitude and latitude) are calculated by spatially interpolating global grid data of UKMO profiles. As for temperature and pressure data in the region higher than those that the UKMO data covers, CIRA86 [*Rees et al.*, 1990] monthly and latitudinal model profiles are used. To connect smoothly the UKMO data and the CIRA model, the CIRA is used above the altitude region 5 km higher than the top altitude where the UKMO data are provided, and the two data sets are interpolated by a cubic spline method for the transition region.

In the data processing that follows, aerosol extinction coefficients at 1-km intervals in tangent height are regarded as unknowns and retrieved. To reduce calculation time, one ray path is selected for each tangent height with 1-km intervals. The selection is made so that the ray path passes a tangent height that is closest to the tangent height of interest.

Figure 1 depicts schematically a spectrum of pseudo-transmittance at 20 km as an example. The spectrum consists of an absorption spectrum caused by oxygen molecules in the center and a continuously varying baseline component, to which aerosol extinction (Mie scattering), scattering due to air molecules (Rayleigh scattering), and absorption due to ozone in the Wulf band contribute. Aerosol extinction at 780 nm is estimated from the average (denoted as τ_b(780 nm) hereafter) of the baseline data obtained by 12 detectors around 780 nm, as shown by the vertical bar in the figure. Note that data contaminated by the Fraunhofer absorption lines are discarded for this calculation. The baseline shape is inferred from the data outside the oxygen molecule absorption spectrum, by applying a functional form expressing an optical depth as a function of wavelength as follows:

$$-\ln(\tau(\lambda)) = a \times \lambda^{-4} + b \times \lambda + c + d \times f(\lambda),$$

where $f(\lambda)$ is an absorption cross section spectrum due to ozone in the Wulf band, which was generated using the MODTRAN subroutine. Since, in this subroutine, temperature dependency is only partly included, the cross section spectrum was calculated at a temperature of 15 °C where no gap happened to appear in the whole spectral region.

The term $d \times f$(780 nm) represents the contribution of the ozone Wulf band. Therefore, by dividing the term τ_b(780 nm) by exp[$-d \times f$(780 nm)], transmittance due only to aerosol extinction and molecular scattering is obtained. Total (aerosol and molecular) extinction coefficients, σ_{am}(780 nm), can be derived by vertically inverting τ_{am}(780 nm). In the version 4.20 procedure the Levenberg-Marquardt technique for the nonlinear least squares method has been used for the vertical inversion of the total extinction coefficients. In the inversion procedure an initial profile is used. However, it has been confirmed that inversion results have little dependency on the initial profile.

Attention should be paid to the fact that the solar radiance decreases from the center of the Sun to the edge (solar limb darkening). Although the size of IFOV is constant, the apparent size of IFOV relative to the Sun when projected onto the Sun surface expands as the tangent height of measurements decreases because the Sun image is "squashed" due to refraction. Therefore limb darkening effects must be considered when calculating theoretical transmittance in inversion processing, especially when the tangent height gets lower than 25 km or so. In the present processing, equation (4) of *Pierce et al.* [1977] is adopted to calculate the limb darkening factor. The IFOV expansion is estimated from refraction calculation in the same way as ray path calculation.

Finally, the aerosol extinction coefficient at each tangent height is obtained by subtracting Rayleigh scattering components from the total (aerosol and molecular) extinction coefficients, σ_{am}(780 nm). The Rayleigh component can be theoretically estimated from the temperature and pressure profile data.

Error information is added to the aerosol extinction data at each tangent height to give error bars. Major error sources contributing to aerosol extinction products are (1) measurement errors due to the instrument characteristics and performance, (2) estimation errors in the Rayleigh scattering component using UKMO data, (3) errors in absorption contribution due to ozone in the Wulf band, (4) error in tangent height estimation, (5) uncertainties of light path length calculation originating in numerical calculations, and (6) errors in calculating the limb darkening effects. As for the measurement errors 1, error propagation in interpolation and extrapolation for 0% and 100% levels is taken into consideration, as well as the effects of level 1 data smoothing. They are calculated for each occultation data stream and stored as "internal error."

The errors in the Rayleigh scattering component come from uncertainty in UKMO data. As the UKMO data are not interpolated in time in the present analysis, a time difference between ILAS measurement and 1200 UT may cause large errors. To verify this, numerical simulation was conducted. Assuming uncertainties of temperature of +/- 2 K at 10 km height and +/- 5 K at 70 km, changes in Rayleigh scattering were calculated for each measurement event. These values for every tangent height were calculated and stored as "external errors" for use in error estimation.

Total error is estimated from the square root of the sum of the squares of the internal and external errors. Since other error sources were not considered in the version 4.20 products, care should be taken in interpreting error bars. The error might be underestimated.

Acknowledgments. We wish to express our great thanks to all of the ILAS science team members and their associates, and especially Hiroshi Kanzawa (NIES), for their efforts with validation experiments. We also thank Mariko Ni nomiya and Hideaki Nakane (NIES) for making their potential vorticity data available. We are also grateful to Richard Swinbank for supplying the UKMO stratospheric assimilation data and trajectory software programs and to Laura Pan (NCAR) for offering the results of ILAS water vapor validation. We also thank Mariko Horikawa for her help with the data plot. The ILAS retrieval data processing was carried out at the ILAS Data Handling Facility (DHF) at NIES.

References

Austin, J., E. E. Remsberg, R. L. Jones, and F. Tuck, Polar stratospheric clouds inferred from satellite data, *Geophys. Res. Lett.*, *13*, 1256-1259, 1986.

Beyerle, G., B. Luo, R. Neuber, T. Peter, and I. S. Mcder mid, Temperature dependence of ternary solution particle volume as observed by lidar in the arctic stratosphere during 1992/1993, *J. Geophys. Res.*, *102*, 3603-3609, 1997.

Browell, E. V., C. F. Butler, S. Ismail, P. A. Robinette, A. F. Carter, N. S. Higdon, O. B. Toon, and M. R. Schoe berl, Airborne lidar observations in the wintertime Arctic stratosphere: Polar stratospheric clouds, *Geophys. Res. Lett.*, *17*, 385-388, 1990.

Burton, S. P., L. W. Thomason, Y. Sasano, and S. Hayashida, Comparison of aerosol extinction measurements by ILAS and SAGE II, *Geophys. Res. Lett.*, *26*, 1719-1722, 1999.

Carslaw, K. S., B. P. Luo, S. L. Clegg, T. Peter, P. Brimble combe, and P. J. Crutzen, Stratospheric aerosol growth and HNO_3 gas phase depletion from coupled HNO_3 and water uptake by liquid particles, *Geophys. Res. Lett.*, *21*, 2479-2482, 1994.

Carslaw, K. S., B. Luo, and T. Peter, An analytic expression for the comparison of aqueous HNO_3-H_2SO_4 stratospheric aerosols including gas phase removal of HNO_3, *Geophys. Res. Lett.*, *22*, 1877-1880, 1995.

Coy, L., E. R. Nash, and P.A. Newman, Meteorology of the polar vortex: Spring 1997, *Geophys. Res. Lett.*, *24*, 2693-2696, 1997.

Deshler, T., B. J. Johnson, and W. R. Rozier, Changes in the character of polar stratospheric clouds over Antarctica in 1992 due to the Pinatubo volcanic aerosol, *Geophys. Res. Lett.*, *21*, 273-276, 1994.

Dye, J. E., D. Baumgardner, B. W. Gandrud, S. R. Kawa, K. K. Kelly, M. Loewenstein, G. V. Ferry, K.R. Chan, and B.L. Gary, Particle size distributions in Arctic polar stratospheric clouds, growth and freezing of sulfuric acid droplets, and implications for cloud formation, *J. Geophys. Res.*, *97*, 8015-8034, 1992.

Fromm, M.D., J. D. Lumpe, R. M. Bevilacqua, E. P. Shettle, J. Hornstein, S.T. Massie, and K. H. Fricke, Observations of Antarctic polar stratospheric clouds by POAM II: 1994-1996, *J. Geophys. Res.*, *102*, 23,659-23,672, 1997.

Hanson, D., and K. Mauersberger, Laboratory studies of the nitric acid trihydrate: Implications for the south polar stratosphere, *Geophys. Res. Lett.*, *15*, 855-858, 1988.

Hervig, M. E., K. S. Carslaw, T. Peter, T. Deshler, L. L. Gordley, G. Redaelli, U. Biermann, and J. M. Russell III, Polar stratospheric clouds due to vapor enhancement: HALOE observations of the Antarctic vortex in 1993, *J. Geophys. Res.*, *102*, 28,185-28,193, 1997.

Iwasaka, Y., T. Hirasawa, and H. Fukunishi, Lidar measurements on the Antarctic stratospheric aerosol layer, I, Winter enhancement, *J. Geomagn. Geoelectr.*, *37*, 1087-1095, 1985.

Koike, M., et al., A comparison of Arctic HNO_3 profiles measured by ILAS and balloon-borne sensors, *J. Geophys. Res.*, *105*, 6761-6771, 2000.

Labitzke, K., and H. van Loon, Trends of temperature and geopotential height between 100 and 10 hPa on the northern hemisphere, *J. Meteorol. Soc. Jpn.*, *72*, 643-652, 1994.

Larsen, N., B. M. Knudsen, J. M. Rosen, N. T. Kjome, R. Neuber, and E. Kyro, Temperature histories in liquid and solid polar stratospheric cloud formation, *J. Geophys. Res.*, *102*, 23,505-23,517, 1997.

Luo, B., U.K. Krieger, and T. Peter, Densities and refractive indices of $H_2SO_4/HNO_3/H_2O$ solutions to stratospheric temperatures, *Geophys. Res. Lett.*, *23*, 3707-3710, 1996.

Massie, S. T., et al., Validation studies using multiwavelength Cryogenic Limb Array Etalon Spectrometer (CLAES) observations of stratospheric aerosol, *J. Geophys. Res.*, *101*, 9757-9773, 1996.

McCormick, M. P., H. M. Steel, P. Hamill, W. P. Chu, and T. J. Swissler, Polar stratospheric cloud sightings by SAM II, *J. Atmos. Sci.*, *39*, 1387-1397, 1982.

McCormick, M. P., and P. H. Wang, Satellite occultation measurements of the Earth's atmosphere using SAM II, SAGE, and SAGE II, *Proc. International School of Physics*, 183-202, 1993.

Nash, E. R., P. A. Newman, J. E. Rosenfield, and M. R. Schoeberl, An objective determination of the polar vortex using Ertel's potential vorticity, *J. Geophys. Res.*, *101*, 9471-9478, 1996.

Newman, P. A., J. F. Gleason, R. D. McPeters, and R. S.

Stolarski, Anomalously low ozone over the Arctic, *Geophys. Res. Lett.*, *24*, 2689-2692, 1997.

Pawson, S., and B. Naujokat, Trends in daily wintertime temperatures in the northern stratosphere, *Geophys. Res. Lett.*, *24*, 575-578, 1997.

Pierce, A. K., C. D. Slaughter, and D. Weinberger, Solar limb darkening in the interval 7404 - 24018 A, II, *Sol. Phy.*, *52*, 179-189, 1977.

Poole, L. R., and M. P. McCormick, Airborne lidar observations of Arctic polar stratospheric clouds: Indications of two distinct growth stages, *Geophys. Res. Lett.*, *15*, 21-23, 1988.

Poole, L. R., and M. C. Pitts, Polar stratospheric cloud climatology based on stratospheric aerosol measurement II observations from 1978 to 1989, *J. Geophys. Res.*, *99*, 13,083-13,089, 1994.

Pullen, S., and R. L. Jones, Accuracy of temperatures from UKMO analyses of 1994/1995 in the arctic winter stratosphere, *Geophys. Res. Lett.*, *24*, 845-848, 1997.

Rees, D.,Barnett, J.J., Labitzke, K. eds., COSPAR International Reference Atmosphere: 1986, part II; Middle Atmosphere Model, *Adv. Space Res.*, *10*, *12*, 519, 1990.

Ricard, P. D., et al., Polar stratospheric clouds as deduced from MLS and CLAES measurements, *Geophys. Res. Lett.*, *22*, 2033-2036, 1995.

Roche, A. E., J. B. Kumer, J. L. Mergenthaler, R. W. Nightingale, W.G. Uplinger, G. A. Ely, and J. F. Potter, Observations of lower-stratospheric $ClONO_2$, HNO_3, and aerosol by the UARS CLAES experiment between January 1992 and April 1993, *J. Atmos. Sci.*, *51*, 2877-2902, 1994.

Sasano, Y., M. Suzuki, T. Yokota, and H. Kanzawa, Improved limb atmospheric spectrometer (ILAS) project: ILAS instrument, performance and validation plan, *J. Soc. Photo Opt. Instrum. Eng.*, *2583*, 193-204, 1995.

Sasano, Y., M. Suzuki, T. Yokota, and H. Kanzawa, Improved Limb Atmospheric Spectrometer (ILAS) for stratospheric ozone layer measurements by solar occultation technique, *Geophys. Res. Lett.*, *26*, 197-200, 1999a.

Sasano, Y., M. Suzuki, T. Yokota, and H. Kanzawa, ILAS for stratospheric ozone layer monitoring: Outline of data processing (version 3.00 and 3.10) and validation experiments, *IEEE Trans. Geosci. Remote Sens.*, *37*, 1508-1516, 1999b.

Sasano, Y., Y. Terao, H.L. Tanaka, T. Yasunari, H. Kan zawa, H. Nakajima, T. Yokota, H. Nakane, S. Hayashida, and N. Saitoh, ILAS observations of chemical ozone loss in the Arctic vortex during early spring 1997, *Geophys. Res. Lett.*, *27*, 213-216, 2000.

Solomon, S., Progress towards a quantitative understanding of Antarctic ozone depletion, *Nature*, *347*, 347-354, 1990.

Stefanutti, L., M. Morandi, M. Del Guasta, S. Godin, and C. David, Unusual PSCs observed by lidar in Antarctica, *Geophys. Res. Lett.*, *22*, 2377-2380, 1995.

Suzuki, M., A. Matsuzaki, T. Ishigaki, N. Kimura, N. Araki, T. Yokota, and Y. Sasano, ILAS, the Improved Limb Atmospheric Spectrometer, on the Advanced Earth Observing Satellite, *IEICE Trans. Fundam Electron. Commun. Comput. Sci.*, *12*, 1560-1570, 1995.

Swinbank, R., and A. O'Neill, A stratosphere-troposphere data assimilation system, *Mon. Weather Rev.*, *122*, 686-702, 1994.

Tabazadeh, A., R. P. Turco, K. Drdla, M.Z. Jacobson, and O.B. Toon, A study of type I polar stratospheric cloud formation, *Geophys. Res. Lett.*, *21*, 1619-1622, 1994.

Tabazadeh, A., O.B. Toon, and P. Hamill, Freezing behavior of stratospheric sulfate aerosols inferred from trajectory studies, *Geophys. Res. Lett.*, *22*, 1725-1728, 1995.

Taylor, F. W., A. Lambert, R.G. Grainger, C.D. Rodgers, and J. J. Remedios, Properties of northern hemisphere polar stratospheric clouds and volcanic aerosol in 1991/92 from UARS/ISAMS satellite measurements, *J. Atmos. Sci.*, *51*, 3019-3026, 1994.

Thomason, L. W., A diagnostic stratospheric aerosol size distribution inferred from SAGE II measurements, *J. Geophys. Res.*, *96*, 22,501-22,508, 1991.

Thomason, L. W., and L. R. Poole, Use of stratospheric aerosol properties as diagnostics of Antarctic vortex processes, *J. Geophys. Res.*, *98*, 23,003-23,012, 1993.

Waibel, A. E., T. Peter, K. S. Carslaw, H. Oelhaf, G. Wetzel, P. J. Crutzen, U. Poschl, A. Tsias, E. Reimer, and H. Fischer, Arctic ozone loss due to denitrification, *Science*, *283*, 2064-2069, 1999.

World Meteorological Organization (WMO), Scientific assessment of ozone depletion, Geneva, 1998.

Yokota, T., M. Suzuki, O.V. Dubovik, and Y. Sasano, ILAS (Improved Limb Atmospheric Spectrometer)/ADEOS data retrieval algorithms, *Adv. Space Res.*, *21*, 393-396, 1998.

S. Hayashida (corresponding author), A. Kagawa, and N. Saitoh, Faculty of Science, Nara Women's University, Nara 630-8506, Japan. (sachiko@ics.nara-wu.ac.jp; kagawa@ics.nara-wu.ac.jp; naoko@leo.ics.nara-wu.ac.jp)

M. Suzuki, Earth Observation Research Center, National Space Development Agency, Tokyo 106-0032, Japan. (suzuki@eorc.nasda.go.jp)

H. Nakajima, Y. Sasano, and T. Yokota, National Institute for Environmental Studies, Tsukuba, Ibaraki 305, Japan. (hide@nies.go.jp; sasano@nies.go.jp; yokota@nies.go.jp)

(Received March 18, 1999; revised April 4, 2000; accepted April 5, 2000.)